Title

Tuft-cell-derived IL-25 regulates an intestinal ILC2—epithelial response circuit

Journal

Nature, 529(7585)

ISSN

0028-0836

Authors

von Moltke, Jakob
Ji, Ming
Liang, Hong-Erh
et al.

Publication Date

2016-01-14

DOI

10.1038/nature16161

Peer reviewed

Published in final edited form as:

Nature. 2016 January 14; 529(7585): 221–225. doi:10.1038/nature16161.

Tuft-cell-derived IL-25 regulates an intestinal ILC2–epithelial response circuit

Jakob von Moltke[1], **Ming Ji**[1,2], **Hong-Erh Liang**[1], and **Richard M. Locksley**[1,2,3]

[1]Department of Medicine, University of California San Francisco, San Francisco, California 94143-0795, USA

[2]Howard Hughes Medical Institute, University of California San Francisco, San Francisco, California 94143-0795, USA

[3]Department of Microbiology & Immunology, University of California San Francisco, San Francisco, California 94143-0795, USA

Abstract

Parasitic helminths and allergens induce a type 2 immune response leading to profound changes in tissue physiology, including hyperplasia of mucus-secreting goblet cells[1] and smooth muscle hypercontractility[2]. This response, known as ‘weep and sweep’, requires interleukin (IL)-13 production by tissue-resident group 2 innate lymphoid cells (ILC2s) and recruited type 2 helper T cells (T_H2 cells)[3]. Experiments in mice and humans have demonstrated requirements for the epithelial cytokines IL-33, thymic stromal lymphopoietin (TSLP) and IL-25 in the activation of ILC2s[4–11], but the sources and regulation of these signals remain poorly defined. In the small intestine, the epithelium consists of at least five distinct cellular lineages[12], including the tuft cell, whose function is unclear. Here we show that tuft cells constitutively express IL-25 to sustain ILC2 homeostasis in the resting lamina propria in mice. After helminth infection, tuft-cell-derived IL-25 further activates ILC2s to secrete IL-13, which acts on epithelial crypt progenitors to promote differentiation of tuft and goblet cells, leading to increased frequencies of both. Tuft cells, ILC2s and epithelial progenitors therefore comprise a response circuit that mediates epithelial remodelling associated with type 2 immunity in the small intestine, and perhaps at other mucosal barriers populated by these cells.

To study the source and regulation of *Il25 in vivo*, we generated a knock-in mouse termed Flare25 (flox and reporter of *Il25; Il25*$^{F25/F25}$) that expresses tandem-dimer red fluorescent

---

Correspondence and requests for materials should be addressed to R.M.L. (locksley@medicine.ucsf.edu).

Online Content Methods, along with any additional Extended Data display items and Source Data, are available in the online version of the paper; references unique to these sections appear only in the online paper.

Supplementary Information is available in the online version of the paper.

Author Contributions J.v.M. conceived the study, designed and performed experiments, analysed data, and wrote the paper with R.M.L. M.J. performed experiments. H.-E.L. cloned the Flare25 reporter cassette, performed the Flare25 embryonic stem cell work, and assisted with additional experiments. R.M.L. directed the study and wrote the paper with J.v.M.

The authors declare no competing financial interests.

Readers are welcome to comment on the online version of the paper.

protein (RFP) from the *Il25* locus and enables conditional deletion of IL-25 activity (Extended Data Fig. 1a). Immunohistochemistry and flow cytometry revealed RFP only in rare epithelial (epithelial cell adhesion molecule (EPCAM)$^+$) cells throughout the digestive tract (Fig. 1a, b and Extended Data Fig. 2). We also found RFP in epithelial cells of the trachea and gall bladder, but not in haematopoietic cells (Extended Data Figs 2 and 3a).

The small intestinal epithelium consists of a single cell layer continuously repopulated from stem cells in underlying crypts; cells progress up the villi and are sloughed into the lumen with a turnover of 3–5 days. Nascent progenitors proliferate in the transit amplifying region before fate commitment to become absorptive enterocytes or, less frequently, one of four secretory cell types: Paneth, enteroendocrine, goblet, or tuft[12,13]. We tested whether Flare25 marks one or more secretory lineages. Immunohistochemistry showed no colocalization of RFP with the enteroendocrine marker chromogranin A (CHGA), the Paneth-cell markers lysozyme (LYZ)1 and LYZ2, or the goblet-cell marker mucin 2 (MUC2) (Fig. 1c and Extended Data Fig. 4a, b). Unexpectedly, expression of RFP and the tuft-cell markers doublecortin-like kinase 1 (DCLK1) and epithelial prostaglandin-endoperoxide synthase 1 (PTGS1) completely overlapped (Fig. 1d and Extended Data Fig. 4a, b). Transcriptional analysis comparing sorted RFP$^+$EPCAM$^+$ with RFP$^-$EPCAM$^+$ intestinal epithelium demonstrated *Il25* expression almost exclusively in RFP$^+$ cells (Fig. 1e), and confirmed co-staining results (Fig. 1f and Extended Data Fig. 3b). The tuft-cell markers *Dclk1*, *Ptgs1*, *Gnat3*, *Chat*, *Gfi1b* and *Trpm5* (ref. 14, 15) were each enriched at least 750-fold in RFP$^+$ cells, while *Chga*, *Muc2*, *Lyz1* and *Lyz2* showed no enrichment (Fig. 1f). Finally, >99% of sorted RFP$^+$EPCAM$^+$ and <1% of RFP$^-$EPCAM$^+$ cells were DCLK1$^+$ by flow cytometry (Fig. 1g). Given these results, and our identification of RFP$^+$ cells only in epithelia where tuft cells have been noted (Extended Data Figs 2 and 4c; data not shown)[14], we conclude that tuft cells constitutively express *Il25* and that all *Il25*$^+$ cells are tuft cells, at least as assessed using this reporter. By contrast, tuft cells are not major sources of TSLP or IL-33 in the small intestine (Extended Data Fig. 5).

Although intestinal tuft cells (also called brush cells) were discovered more than 50 years ago, their function remains largely unknown. Given the link between IL-25 and type 2 immunity, we investigated the role of tuft cells during infection of mice with the roundworm *Nippostrongylus brasiliensis*, which induces a strong type 2 immune response that clears intestinal worms 7–10 days post-infection (d.p.i.). Although tuft cells account for <1% of intestinal epithelium in uninfected mice, we found dramatic (>15-fold) tuft cell hyperplasia in the small intestine 7 d.p.i. (Fig. 2a–c). The extent of hyperplasia was uniform throughout the small intestine (Extended Data Fig. 6), but we focused further experiments on the duodenum and jejunum, where *N. brasilienesis* resides. We observed no hyperplasia in the stomach or colon (Extended Data Fig. 6), through which the worms briefly transit. Hyperplasia in the small intestine peaked 8–9 d.p.i. and returned to near homeostatic levels by 14 d.p.i. (Fig. 2d). As in uninfected mice, RFP$^+$ cells were CHGA$^-$, MUC2$^-$ and LYZ1/2$^-$, and DCLK1$^+$ and PTGS1$^+$ 7 d.p.i. (Extended Data Fig. 7). Given the complete overlap of RFP and DCLK1, we used these markers interchangeably in further experiments.

Since helminth-induced goblet cell hyperplasia is mediated by IL-13 (ref. 16), we asked whether IL-13 also mediates tuft cell hyperplasia. Indeed, tuft cell hyperplasia was absent in

infected interleukin 4 receptor α (*Il4ra*)-deficient mice, in which both IL-4 and IL-13 signalling is disrupted, and in *Il13* deleter mice (*Il13*$^{cre/cre}$; *Gt(ROSA)26*$^{STOP\text{-}flox::DTA/+}$) (Fig. 2e). Because tuft cell hyperplasia was normal in IL-4-deficient mice (*Il4*$^{KN2/KN2}$) (Fig. 2e), and because the predominant role of IL-13 in IL-25-mediated pathologies is well established[17,18], we conclude that IL-13 is the primary signal driving tuft cell hyperplasia *in vivo*. We also found *Il4/13*-dependent tuft cell hyperplasia after infection with *Heligmosomoides polygyrus*, another intestinal parasite (Extended Data Fig. 7c).

Lamina propria ILC2s are the principal intestinal source of IL-13 in the first week of *N. brasiliensis* infection[19,20]. Accordingly, tuft cell hyperplasia was absent or reduced 7 d.p.i. in mice lacking nearly all lymphoid cells (*Il7ra*$^{-/-}$, *Il2rg*$^{-/-}$) or IL-5^{+} ILC2 cells (*Il5* deleter: *Il5*$^{cre/cre}$;*Gt(ROSA)26*$^{STOP\text{-}flox::DTA/STOP\text{-}flox::DTA}$) (Fig. 2e). Hyperplasia was greatly reduced in *Rag1*$^{-/-}$ mice, but nearly normal in *Il4/13*$^{fl/fl}$; *Cd4-cre* mice (Fig. 2e), consistent with the model that T cells produce little IL-13 at early time points but can boost IL-13 levels by supporting ILC2 activation[21].

To test if type 2 cytokines are sufficient to induce tuft cell hyperplasia, we injected mice with stabilized IL-4–anti-IL-4 complexes that mimic IL-13 signalling, or with IL-25 or IL-33. All three treatments expanded tuft cells, but the effects of IL-25 and IL-33 were IL4RA-dependent and severely reduced in the absence of lymphoid cells (*Il7ra*$^{-/-}$, *Il2rg*$^{-/-}$), *Il5*$^{+}$ cells, or *Il13*$^{+}$ cells (Fig. 2f, g), suggesting that IL-25 and IL-33 trigger hyperplasia indirectly by inducing IL-13 production in ILC2s. By contrast, tuft cell hyperplasia was reduced only partially in *Il7ra*$^{-/-}$ and *Il2rg*$^{-/-}$ mice injected with IL-4 (Fig. 2h), raising the possibility that exogenous IL-4 or endogenous IL-13 induces tuft cell hyperplasia by directly targeting the epithelium.

Consistent with this model, recombinant IL-4 and IL-13 induced tuft cell hyperplasia in intestinal organoids, which contain only epithelial cells; by contrast, IL-25 and IL-33 neither induced hyperplasia nor enhanced induction by IL-4/IL-13 in this system (Fig. 3a and Extended Data Fig. 3c, d). As expected, tuft cell hyperplasia was absent in *Il4ra*$^{fl/fl}$; *Vil1-cre* mice, confirming that tuft cell hyperplasia requires IL4RA signalling in the intestinal epithelium *in vivo* (Fig. 3b). We conclude that ILC2-derived IL-13 signals through IL4RA in the intestinal epithelium to induce tuft cell hyperplasia.

We examined several possible mechanisms of IL-13-induced tuft cell hyperplasia. First, CHGA^{+} cell numbers did not change during infection (Extended Data Fig. 8b, c), confirming a selective increase in tuft cells rather than a global expansion of intestinal epithelium. Through lineage tracing, we confirmed that tuft cells, as under resting conditions, continue to arise from *Lgr5*$^{+}$ stem cells during *N. brasiliensis*-induced hyperplasia (Fig. 3c). Since *Il4ra* is expressed throughout the intestinal epithelium[22,23], tuft cell expansion could occur either before or after lineage commitment; however, we found expression of the proliferation marker Ki67 in only a few nascent tuft cells (Fig. 3d), suggesting that tuft cell hyperplasia is induced in the stem or transit amplifying compartments. Consistent with this model, kinetic studies revealed a wave of hyperplastic tuft cells appearing near the crypts 6 d.p.i. and moving up the villi by 8 d.p.i. (Fig. 3e). Taken together, these results suggest that IL-13 signalling in uncommitted intestinal

epithelium shifts cell fate decisions towards the tuft (and goblet) cell lineage, perhaps by altering the balance of Notch signalling[12]. Indeed, the Notch signalling inhibitor *N*-[*N*-(3,5-Difluorophenacetyl)-3-alanyl]-*S*-phenylglycine *t*-butyl ester (DAPT) also induced tuft cell hyperplasia in organoids (Extended Data Fig. 3e–f).

Since ILC2s secrete IL-13 in response to IL-25, and tuft cells are the source of intestinal IL-25, we hypothesized a feed-forward circuit between tuft cells, ILC2s, and epithelial progenitors (Extended Data Fig. 8d). Tuft cells constitutively express *Il25* (Fig. 1a, e) and some lamina propria ILC2s constitutively express *Il13* (ref. 24), so we first examined the interaction of tuft cells and ILC2s in uninfected mice. Using $Il13^{Smart/Smart}$ reporter mice to mark IL-13-secreting cells, we found that ~20% of lamina propria ILC2s make IL-13 in the absence of infection, and this is dependent on IL-25 (Fig. 4a and Extended Data Fig. 9a). The frequency of ILC2s is also decreased in $Il25^{-/-}$ mice (Fig. 4b), suggesting that tuft-cell-derived IL-25 promotes ILC2 maintenance in the small intestine. ILC2 activation remains IL-25-dependent at 4 d.p.i., the latest time point before worm clearance at which we could recover viable cells from infected intestines (Fig. 4a and Extended Data Fig. 9a). T_H2 cells are not a major source of IL-13 at rest or 4 d.p.i. (Extended Data Fig. 9b, c).

Our model of an ILC2–epithelial circuit predicts that loss of homeostatic IL-25 or IL-13 would reduce the frequency of tuft cells. Indeed, the already small number of tuft cells was further reduced in uninfected $Il25^{-/-}$ and $Il4ra^{-/-}$ mice (Fig. 4c), with the remaining tuft cells in these mice probably representing stochastic production independent of type 2 immunity. The frequency of $CHGA^+$ cells was unchanged in $Il25^{-/-}$ mice (Extended Data Fig. 8b, c). We generated $Il25^{F25/F25}$*;Vil1-cre* mice to delete *Il25* selectively from the epithelium (Extended Data Fig. 1b, c). The basal frequency of tuft cells again decreased (Fig. 4d), confirming that tuft cells are the relevant source of IL-25 upstream of homeostatic production of IL-13 by intestinal ILC2s.

The dependence of tuft cell frequency on autocrine IL-25 was even more striking during *N. brasiliensis* infection. Tuft cell hyperplasia was absent in $Il25^{-/-}$ and $Il25^{F25/F25}$*;Vil1-cre* mice 7 d.p.i., but unaffected by the absence of TSLP or IL-33 signalling (Fig. 4e, f). Taken together, our data support a model in which IL-25 from tuft cells induces ILC2s to produce IL-13, which in turn regulates the frequency of tuft cells in the intestinal epithelium. The capacity of IL-13 to alter the cellular composition of the epithelium raised the possibility that tuft cells might also regulate other secretory lineages. While neither $CHGA^+$ nor Paneth cell hyperplasia occurred during worm infection (Extended Data Fig. 8a–c), goblet cell hyperplasia and hypertrophy were absent in infected mice lacking epithelial IL-25 (Fig. 4g–i). Moreover, as in $Il25^{-/-}$ mice, $Il25^{F25/F25}$*;Vil1-cre* mice failed to clear worms by 10 d.p.i., thereby identifying tuft cells as key regulators of the type 2 immune response (Fig. 4j).

Our findings uncover an unexpected role for tuft cells in intestinal immune defence, suggest a link between type 2 immune signalling and epithelial cell fate decisions, and describe an ILC2–epithelial response circuit that regulates the cellular composition of the intestinal epithelium. This circuit could integrate homeostatic signals, such as ILC2 activation during feeding[24], with additional signals to tune the barrier's absorptive–secretory balance. Indeed, despite the feed-forward nature of the circuit, tuft and goblet cell hyperplasia are restrained

during homeostasis, suggesting that worm infection provides another activating signal or removes an inhibitory signal. Given their positioning in the intestinal epithelium, tuft cells appear poised to monitor luminal homeostasis and transduce activating signals to immune cells in the lamina propria. Interestingly, tuft cells encode the complete bitter and umami taste transduction pathways and release acetylcholine when activated[14]. In the airways and urethra, this pathway has been linked to smooth muscle contraction and is proposed to promote innate defence against invading bacteria[25–28].

In the absence of IL-25, other signals such as IL-33 become induced[5] and can activate ILC2s to mediate expansion of tuft and goblet cells associated with worm clearance. Nonetheless, our findings delineate a key role for tuft cells in the physiological host response to helminths. Tuft cells appear to be the primary source of IL-25 in the lung as well (Extended Data Fig. 4c); thus, their involvement may extend to other conditions in which IL-25 has been implicated, such as airway disease[11,29] and allergic diarrhoea[30]. Indeed, mucosal tuft cell hyperplasia may be a generalizable hallmark of type 2 immune responses, and strategies to short-circuit tuft cell activation may have therapeutic potential for these widespread afflictions.

METHODS

Il25 reporter mice

Flare25 mice were generated by homologous gene targeting in C57BL/6 embryonic stem cells. A 2.2 kb 3′ homology arm beginning in the 3′3UTR of *Il25* was amplified from C57BL/6 genomic DNA and cloned into pKO915-DT (Lexicon Genetics) using BamHI and HindIII. Next, a DNA strand encoding (from 5′ to 3′) a *loxP* site and the complete third exon of *Il25* was synthesized (Blue Heron). This synthetic strand and genomic DNA were used as PCR templates to generate a 2.1 kb 5′ homology arm by overlap extension PCR. The 5′ homology arm was cloned into the pK0915-DT vector containing the 3′ homology arm using XhoI and EcoRI. Finally, a reporter cassette encoding (in order from 5′ to 3′): a *loxP* site, encephalomyocarditis virus IRES, tandem RFP, bovine growth hormone poly(A), and a frt-flanked neomycin resistance cassette, was subcloned into the homology arm containing pKO915-DT vector using AscI. The final construct was linearized with NotI and transfected by electroporation into C57BL/6 embryonic stem cells. Cells were grown on irradiated feeders with the aminoglycoside G418 in the media, and neomycin-resistant clones were screened for 5′ and 3′ homologous recombination by PCR. Four positive clones were selected and further tested to confirm insertion of the 5′*loxP* site. Two clones were selected for injection into albino C57BL/6 blastocysts to generate chimaeras, and the male pups with highest ratios of black-to-white coat colour from a single clone were selected to breed with homozygous Gt(ROSA26)$^{FLP1/FLP1}$ females (Jackson Laboratories catalogue no. 009086) to excise the neomycin resistance cassette. Deletion of neomycin was confirmed by PCR. Flare25 genotyping primers were as follows: KI_F: GTATTGGGTGCCAGAACAG; KI_R: GGGTCGCTACAGACGTTGTTTGTC (715 bp knock-in band; 374 bp floxed band); WT_F: ACTTTACCACAACCAGACG; WT_R: AGTTTCTCCCCAAGTCCTCC (290 bp wild-type band).

Other mice

Mice were maintained in the University of California San Francisco (UCSF) specific pathogen-free animal facility in accordance with the guidelines established by the Institutional Animal Care and Use Committee and Laboratory Animal Resource Center. All experimental procedures were approved by the Laboratory Animal Resource Center at the UCSF. Mice aged 6–12 weeks were used for all experiments. Mice were age- and sex-matched in figures displaying a single representative experiment. Pooled results include both male and female mice. For some experiments, mice encoding a reporter allele that does not impact endogenous gene expression (B6.*Il13*^{Smart} or B6.*Arg1*^{YARG}) were used as wild-type controls. *Il7ra*$^{-/-}$ (B6.129S7- Il7r^{tm1Imx}/J; 002295), *Rag1*$^{-/-}$ (B6.129S7-Rag1^{tm1Mom}/J; 002216), *Cd4-cre* (B6.Cg-Tg(Cd4-cre); 022071) and wild-type (C57BL/6J; 000664) mice were purchased from Jackson Laboratories. *Il4ra*$^{-/-}$ (BALB/c-Il4ra^{tm1Sz}/J; 003514) mice were purchased from Jackson Laboratories and backcrossed to C57BL/6J for at least eight generations. *Il2rg*$^{-/-}$ (B10;B6-Il2rg^{tm1Wjl}; 4111-F) were purchased from Taconic as *Rag-2*$^{-/-}$;*Il2rg*$^{-/-}$ and outcrossed to isolate the *Il2rg* allele. B6.*Il25*$^{-/-}$, *B6.Tslpr*$^{-/-}$, *B6.Il33r*$^{-/-}$, B6.*Il13*$^{Smart/Smart}$, B6.*Il4*$^{KN2/KN2}$, *B6.Il5*$^{cre/cre}$;*Gt(ROSA)26*$^{STOP\text{-}flox::DTA/STOP\text{-}flox::DTA}$ and B6.*Il13*$^{cre/cre}$; *Gt(ROSA)26*$^{STOP\text{-}flox::DTA/+}$ mice were obtained or generated as described[9,19,24]. BALB/c.*Il4/13*$^{fl/fl}$ mice were generated as described[20] and backcrossed to C57BL/6J for at least eight generations. B6.*Il4ra*$^{fl/fl}$ mice were provided by A. Chawla. B6.*Tg(Vil1-cre)* mice were provided by A. Ma. B6.*Lgr5*$^{Egfp::cre\text{-}Ert2/+}$; *Gt(ROSA)26*$^{STOP\text{-}flox::RFP/+}$ mice were provided by O. Klein.

Mouse infection and treatment

Infectious third-stage *N. brasiliensis* larvae (L3) were raised and maintained as described[19]. Mice were infected subcutaneously with 500 *N. brasiliensis* L3 or by oral gavage with 200 *H. polygyrus* L3, and were killed at the indicated time points to collect tissues for staining or to count intestinal worm burden, as described[19]. Mice were given IL-4, IL-25, and IL-33 as follows: IL-4 complexes were generated by incubating 2 μg mouse IL-4 (R&D Systems) with 10 μg LEAF purified anti-mouse IL4 antibody (clone 11B11, Biolegend) for 30 min at room temperature, and then administered on day 0 and day 2. IL-25 and IL-33 were given in doses of 500 ng on days 0, 1, 2, and 3. All injections were given intraperitoneally in 200 μl, and all intestines were harvested for sectioning and staining on day 4. For lineage tracing, 2.5 mg of tamoxifen in 250 μl corn oil were given intraperitoneally 5 days before harvest.

Fixed tissue preparation and staining

For immunohistochemistry, tissues were fixed in 4% paraformaldehyde for 3 h at 4 °C followed by PBS wash and overnight incubation in 30% (w/v) sucrose. For stomach, small intestine, caecum and large intestine, tissues were flushed with PBS before fixation. Unless otherwise noted, the proximal 10–12 cm of small intestine (duodenum and partial jejunum) were harvested. Tissues were embedded in Optimal Cutting Temperature Compound (Tissue-Tek) and stored at −80 °C before sectioning (8–10 μm) on a Cryostat (Leica). To facilitate analysis of the entire sample, small and large intestines were coiled into a ‘Swiss roll’ before embedding.

Immunohistochemistry was performed in Tris/NaCl blocking buffer (0.1 M Tris-HCl, 0.15 M NaCl, 5 μgml^{-1} blocking reagent (Perkin Elmer), pH 7.5) as follows: 1 h 5% goat serum, 1 h primary antibody, 40 min secondary antibody, 5 min DAPI (Roche). For RFP co-labelling experiments, slides were stained for MUC2, LYZ1, CHRA, or DCLK1 as described above, excluding the DAPI step. RFP staining was then as follows: 1 h rabbit IgG, 20 min each of biotin and streptavidin block (Vector Labs), 1 h anti-RFP-biotin, 40 min streptavidin-Cy3 (Caltag), and 5 min DAPI. See Extended Data Table 1 for a list of antibodies used in this study.

For goblet cell staining, 8-cm sections of jejunum were fixed for 3 h in 10% buffered formalin (Fisher Scientific) at 4 °C before coiling into a 'Swiss roll' and returning to formalin. After 24 h, tissues were moved to 70% ethanol for storage. Tissue processing, paraffin embedding, and sectioning were performed by the UCSF Mouse Pathology Core. Periodic acid Schiff (PAS) and Alcian blue staining were performed as follows: cleared with xylenes (Fisher Scientific), rehydrated, 30 min in Alcian blue (Thermo Scientific), 5 min in periodic acid (Thermo Scientific), 15 min in Schiff reagent (Thermo Scientific), dehydrated, and mounted. Brightfield and fluorescent images were acquired with an AxioCam HR camera on an AxioImagerM2 upright microscope (Zeiss).

Tuft and goblet cell quantification

In uninfected mice, a 2.5-cm section of small intestine was harvested beginning 10 cm distal to the stomach and processed into a single-cell epithelial suspension as described later. After analysis by flow cytometry, frequency of tuft cells was calculated as number of DCLK1^{+}EPCAM^{+} cells/total number of EPCAM^{+} cells. Because viable epithelial cells cannot be harvested from *N. brasiliensis*-infected intestines from ~5 to ~12 d.p.i., immunohistochemistry was used to quantify tuft cell frequency in infected mice. The proximal 10 cm of small intestine were harvested and stained for DCLK1 as described earlier. A 4 ×4 grid of images was collected at ×200 magnification and the total area of DCLK1 and DAPI staining above background was calculated using ImageJ. Tuft cell frequency was calculated as DCLK1 staining area/DAPI staining area.

For goblet cell quantification, tissue sections were prepared and stained with PAS Alcian blue as described earlier. Goblet cells were manually counted and the total length of all analysed villi was measured using ImageJ. Goblet cell frequency was expressed as number of goblet cells/millimetre of villus. At least 15 villi were counted for each replicate. Mucus production was estimated by measuring the area of at least 15 goblet cells for each biological replicate.

Single-cell tissue preparation

For single-cell epithelial preparations, small intestines were flushed with PBS, opened, and rinsed with PBS to remove luminal contents. Two-and-a-half- to five-cm-long segments of jejunum were incubated with rocking for 20 min at 37 °C in 5 ml PBS containing 2.5 mM EDTA (Sigma-Aldrich), 0.75 mM dithiothreitol (DTT; Sigma-Aldrich), and 10 μgml^{-1} DNaseI (Sigma-Aldrich). Tissues were shaken vigorously for 30 s and released cells were incubated with rocking for 10 min at 37 °C in 5 ml HBSS (Ca^{2+}/Mg^{2+} free) containing 1.0

U ml^{-1} Dispase (Gibco) and 10 $\mu g ml^{-1}$ DNaseI. Digested cells were passed through a 70 μm filter and washed once before staining for flow cytometry.

For lamina propria preparations, small intestine was harvested from 4–10 cm distal to the stomach (duodenum/jenunum), flushed with PBS, opened, and thoroughly cleaned with PBS. Intestines were incubated with gentle rocking for 15 min at 37 °C in 10 ml HBSS (Ca^{2+}/Mg^{2+} free) supplemented with 5% fetal calf serum (FCS), 10 mM HEPES (UCSF Cell Culture Facility), 10 mM DTT and 5 mM EDTA. Intestines were gently vortexed, supernatants discarded, and incubation repeated with fresh DTT/EDTA solution. Next, intestines were incubated with gentle rocking for 20 min at 37 °C in 20 ml HBSS (Ca^{2+}/Mg^{2+} replete) supplemented with 5% FCS and 10 mM HEPES. After incubation, intestines were gently vortexed, cut into small pieces and incubated with gentle rocking for 30 min at 37 °C in 5 ml HBSS (Ca^{2+}/Mg^{2+} replete) supplemented with 5% FCS, 10 mM HEPES, 30 $\mu g ml^{-1}$ DNaseI, and 0.1 Wunsch ml^{-1} LiberaseTM (Roche). After digest, intestines were mechanically dissociated in GentleMACS C tubes (Miltenyi Biotec), passed through a 70 μm filter, and washed. The resulting cell pellet was resuspended in 4 ml 40% Percoll (Sigma-Aldrich), underlaid with 4 ml 90% Percoll and centrifuged at 2,200 r.p.m. for 20 min at 4 °C. The 40/90 interphase of the Percoll gradient was harvested, washed, and stained for flow cytometry.

Flow cytometry

For surface staining, single-cell suspensions prepared as described earlier were incubated with anti-CD16 and CD32 monoclonal antibodies (UCSF Antibody Core Facility) for 10 min at 4 °C. The cells were stained with antibodies to surface markers for 20 min at 4 °C followed by DAPI for dead cell exclusion. See Extended Data Table 1 for a list of antibodies used in this study.

For intracellular DCLK1 staining, single-cell epithelial suspensions were prepared from 2.5 cm sections of small intestine harvested 8 cm distal to the stomach. Staining was as follows: 15 min at 4 °C in Violet Live/Dead fixable stain (Life Technologies), 15 min at room temperature in 2% paraformaldehyde (Electron Microscopy Sciences), 20 min at room temperature in saponin-based permeabilization and wash (perm/wash) reagent (Life Technologies) supplemented with 10% goat serum, 30 min with rabbit anti-doublecortin-like kinase (Abcam; ab31704) in perm/wash, 20 min in F(ab′)2 goat anti-rabbit IgG-Alexa Fluor 488 (Life Technologies) and rat anti-EPCAM-PerCP-Cy5.5 (Biolegend; 16A8). For intracellular GATA3 staining, single-cell lamina propria suspensions were prepared from the small intestines as described earlier and stained according to manufacturer's protocol for FoxP3/Transcription Factor Staining Buffer Set (eBiosciences).

Samples were analysed on an LSR II (BD Biosciences) with four lasers (403 nm, 488 nm, 535 nm, and 633 nm). Samples were FSC-A/SSC-A gated to exclude debris, FSC-W/FSC-A gated to select single cells, and gated to exclude $DAPI^{+}$ dead cells. Data were analysed with FlowJo 10 (Treestar).

Quantitative RT–PCR

Single-cell epithelial suspensions were isolated and stained as described earlier and then sorted into $RFP^{+}EPCAM^{+}$ and $RFP^{-}EPCAM^{+}$ populations using a MoFlo XDP (Beckman Coulter). RNA was isolated using the Micro Plus RNeasy kit (Qiagen) and reverse transcribed using the SuperScript Vilo Master Mix (Life Technologies). The resulting cDNA was used as template for quantitative PCR with the Power SYBR Green reagent on a StepOnePlus cycler (Applied Biosystems). Transcripts were normalized to *Rps17* (40S ribosomal protein S17) expression. See Extended Data Table 1 for a list of primers used in this study.

Organoid culture

Small intestinal crypt-derived organoids were grown as described[31], replacing recombinant R-spondin with supernatants from R-spondin expressing L-cells (provided by O. Klein). Crypts were harvested from $Il25^{F25/F25}$ mice and plated on day 0. On day 3 and day 5, media were replaced and organoids were treated with 20 ng ml^{-1} of the indicated recombinant protein. On day 6 organoids were harvested into HBSS (Ca^{2+}/Mg^{2+} replete) containing 200 U ml^{-1} Collagenase I (Gibco) and 1.8 U ml^{-1} Dispase (Gibco). Organoids were incubated for 1.5 h at 37 °C with shaking, washed, and then stained for flow cytometry as described earlier.

Statistical analysis

All experiments were performed using randomly assigned mice without investigator blinding. All data points and *n* values reflect biological replicates (that is, mice), except in Fig. 3a, where data points on the graph represent technical replicates. No data were excluded. Where noted in the figures, statistical significance was calculated without assumption of normal distribution using a Mann–Whitney test. Experimental groups included a minimum of three biological replicates, as required by the Mann–Whitney test. Intragroup variation was not assessed. All statistical analysis was performed using Prism 6 (GraphPad Software). Figures display means ± s.e.m. No statistical methods were used to predetermine sample size.

Extended Data

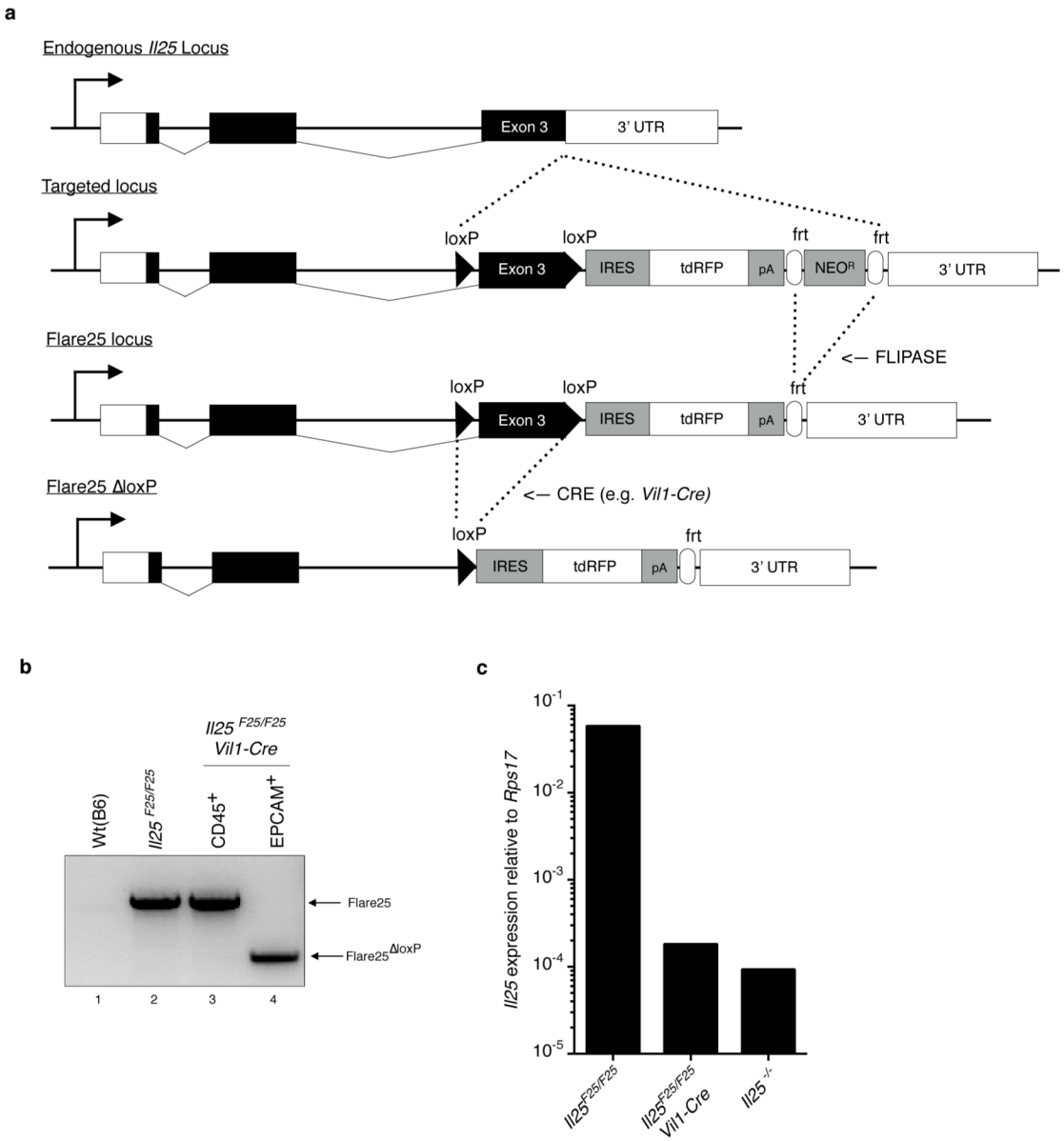

Extended Data Figure 1. Flare25 mouse and *Vil1-cre*-mediated *Il25* deletion

a, Gene-targeting strategy for the flox and reporter of *Il25* (Flare25) mouse. **b**, PCR of genomic DNA isolated from the tail (lane 1, 2) or cells sorted from the small intestine (lane 3, 4) of indicated mice. **c**, Quantitative RT–PCR for *Il25* on cDNA from EPCAM$^+$ cells sorted from the small intestine of indicated mice. **b**, **c**, Data are representative of two experiments (n = 2). Frt, target site for FLIPASE recombinase; IRES, internal ribosomal entry site; *loxP*, target site for Cre recombinase; pA, bovine growth hormone poly(A) tail; tdRFP,3tandem-dimer red fluorescent protein; UTR, untranslated region. For gel source data (**b**) see Supplementary Fig. 1.

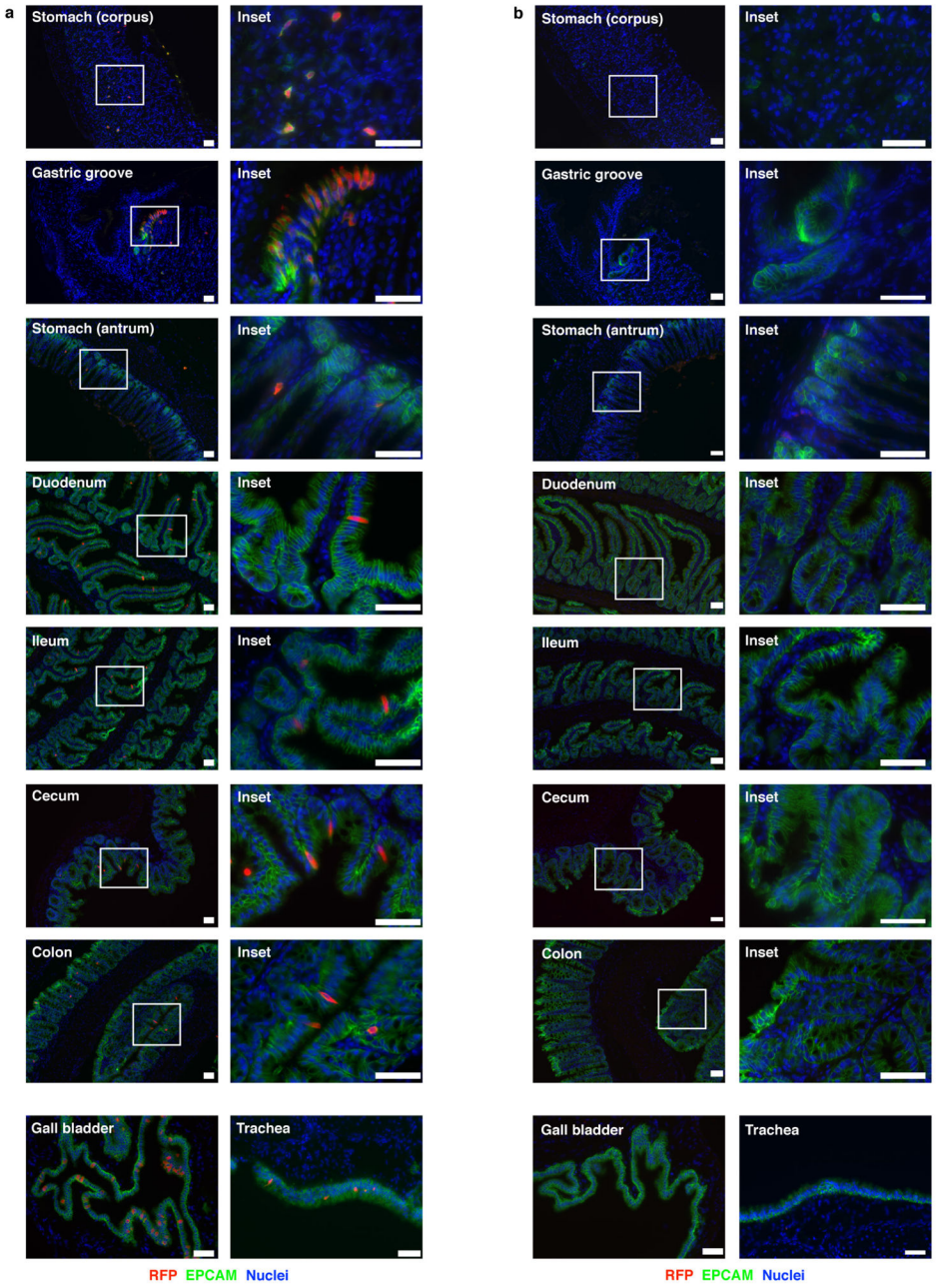

Extended Data Figure 2. *Il25* expression in epithelial surfaces

a, **b**, Indicated tissues of *Il25*$^{F25/F25}$ (**a**) and wild-type control (**b**) mice stained by immunohistochemistry for RFP (red), EPCAM (green), and DAPI (blue). Some data from Fig. 1a are repeated here to allow complete comparison. Scale bars, 50 μm. Images are representative of at least three independent experiments. n =3.

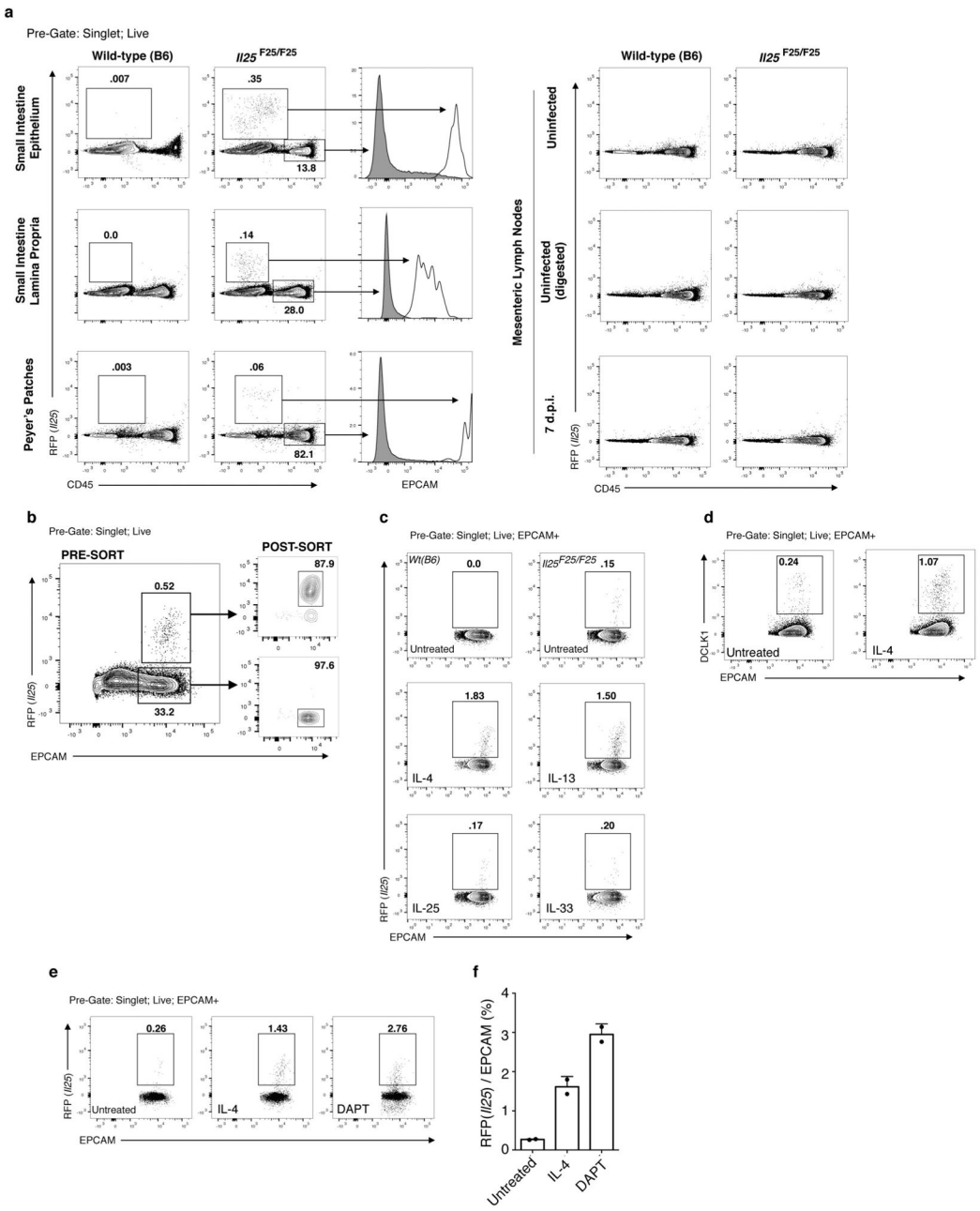

Extended Data Figure 3. Flow cytometry gating strategies and organoid culture

a, Flow cytometric analysis of indicated tissues in *Il25*$^{F25/F25}$ and wild-type mice. **b**, Flow cytometric analysis of small intestine epithelial cells of *Il25*$^{F25/F25}$ mice before and after fluorescence-activated cell sorting (FACS) into RFP^{+}EPCAM^{+} and RFP^{-}EPCAM^{+} pools for analysis by quantitative RT–PCR. **c**–**e**, Representative flow cytometric analysis of small-intestine-derived organoids from *Il25*$^{F25/F25}$ (**c**–**e**) and wild-type (**c**) mice cultured with or without recombinant protein (20 ng ml^{-1}), as indicated (**c**–**e**) or Notch signalling inhibitor DAPT (25 μM) (**e**). Single-cell suspensions of the organoids were stained for EPCAM (**c**–**e**) and DCLK1 (**d**), and gated to quantify tuft cell (RFP^{+}EPCAM^{+} or DCLK1^{+}EPCAM^{+})

frequency. **f**, Quantification of two technical replicates from experiment shown in **e**. d.p.i., days post-*N. brasiliensis* infection. Data in **f** are technical replicates. Data are representative of three (**a**, **b**, **d**) or two (**c**, **e**, **f**) independent experiments. In **a**–**d**, n =3; in **e**, **f**, n =2. Error bars represent mean ±s.e.m.

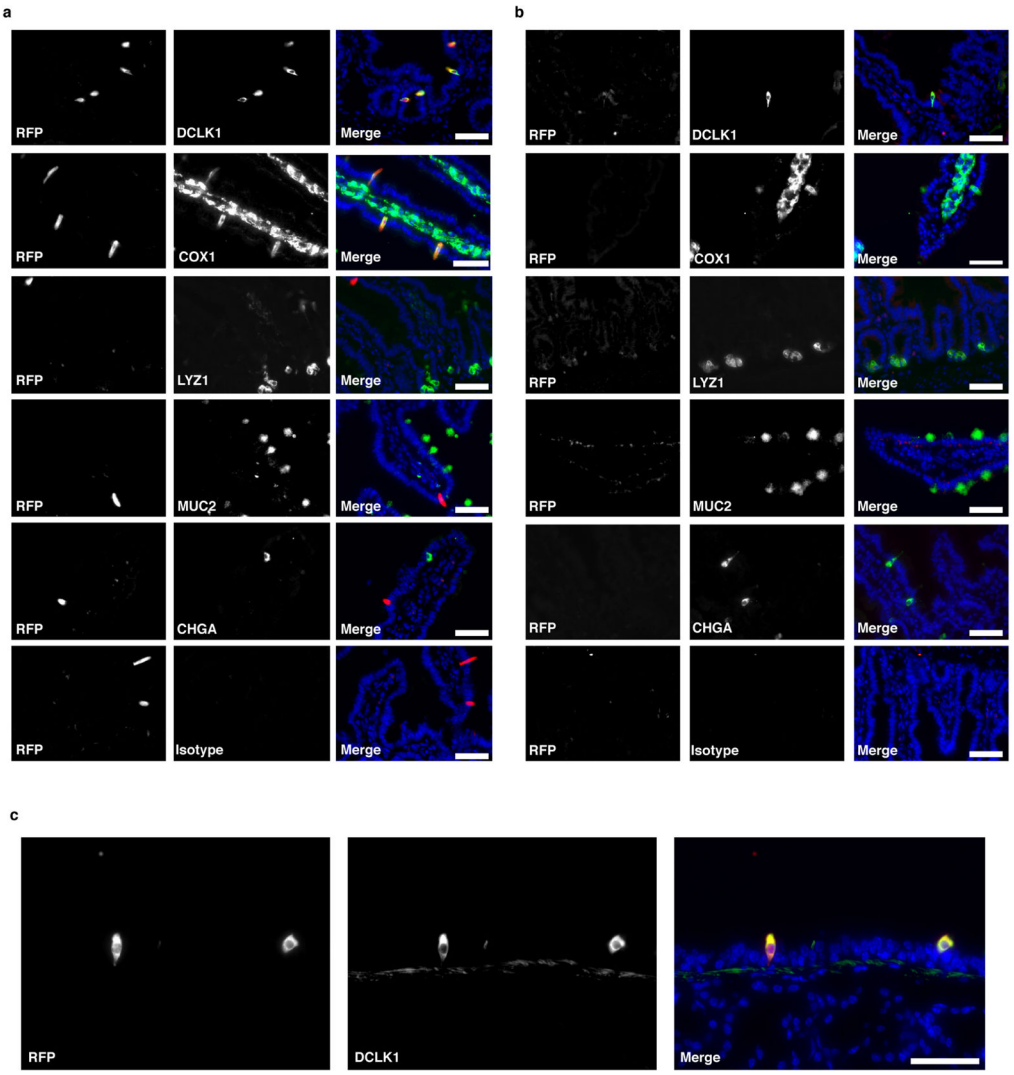

Extended Data Figure 4. *Il25* is expressed constitutively in tuft cells

a–**c**, Jejunum (**a**, **b**) or trachea (**c**) of *Il25*$^{F25/F25}$ (**a**, **c**) and wild-type control (**b**) mice stained by immunohistochemistry for RFP (red), indicated lineage markers (green), and DAPI (blue). Scale bars, 50 μm. Images are representative of one (**c**) or two (**a**, **b**) independent experiments. n =2.

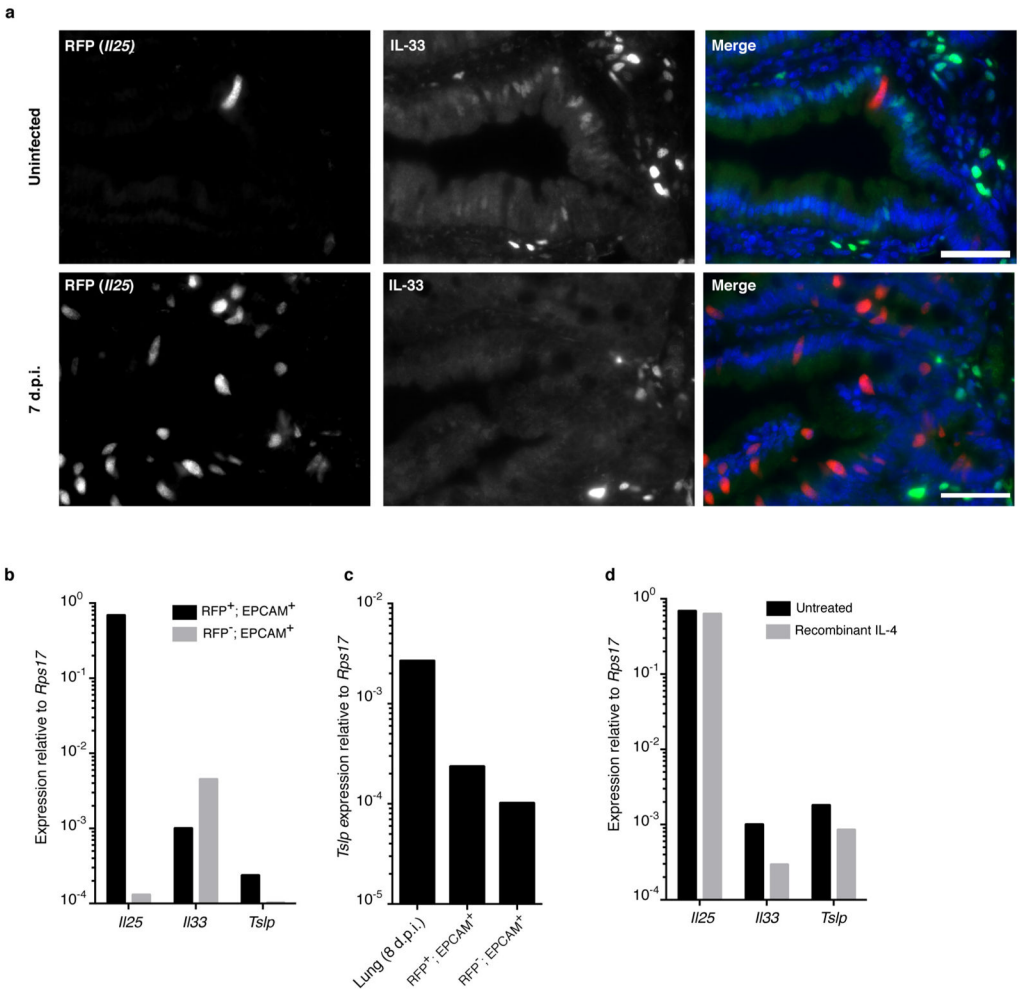

Extended Data Figure 5. Tuft cells are not a major source of intestinal TSLP or IL-33

a, Jejunum of *Il25*$^{F25/F25}$ mice stained for RFP (red), IL-33 (green), and DAPI (blue). **b**–**d**, Quantitative RT–PCR on indicated (**b**, **c**) or RFP^{+}EPCAM^{+} (**d**) cells sorted from untreated (**b**, **c**) mice or mice treated as indicated (**d**). RNA isolated from whole lung 8 days post-*N. brasiliensis* infection is used as a positive control for *Tslp* expression in **c**. Expression of *Tslp* in sorted *Tslp*-expressing cells of the lung would probably be higher. Scale bars, 50 μm. Data are representative of two independent experiments. In **a**, n =3; in **b**–**d**, n =2.

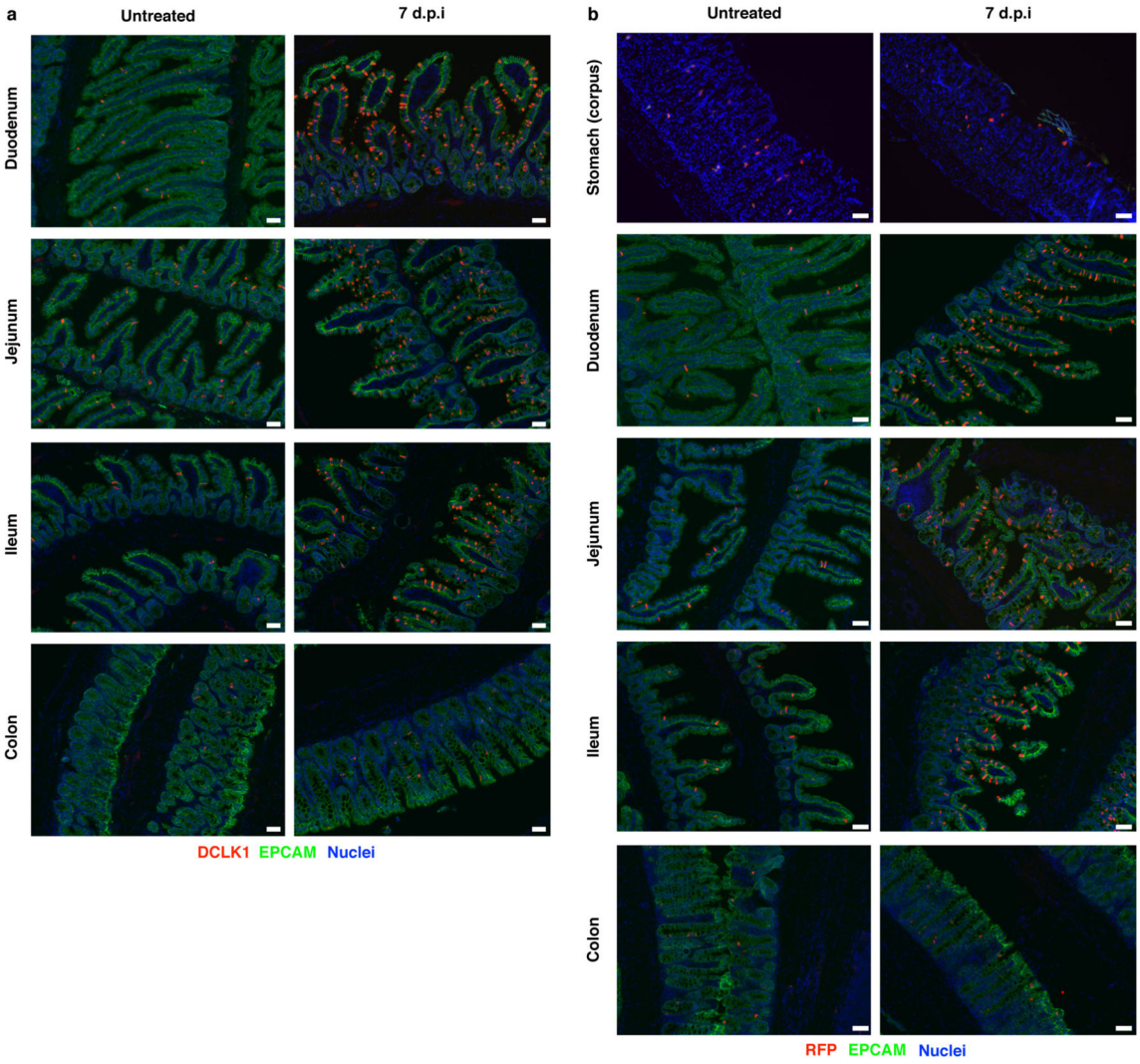

Extended Data Figure 6. *N. brasiliensis* induces tuft cell hyperplasia throughout the small intestine but not in stomach and colon

a, **b**, Indicated tissues of *Il25*$^{F25/F25}$ (**a**) and wild-type control (**b**) mice treated as indicated and stained by immunohistochemistry for RFP (**a**) or DCLK1 (**b**) (red), EPCAM (green), and DAPI (blue). d.p.i., days post-*N. brasiliensis* infection. Scale bars, 50 μm. Data are representative of two (stomach and colon) or at least three (all others) independent experiments. In **a**, stomach and colon: $n = 2$; all others: $n > 5$.

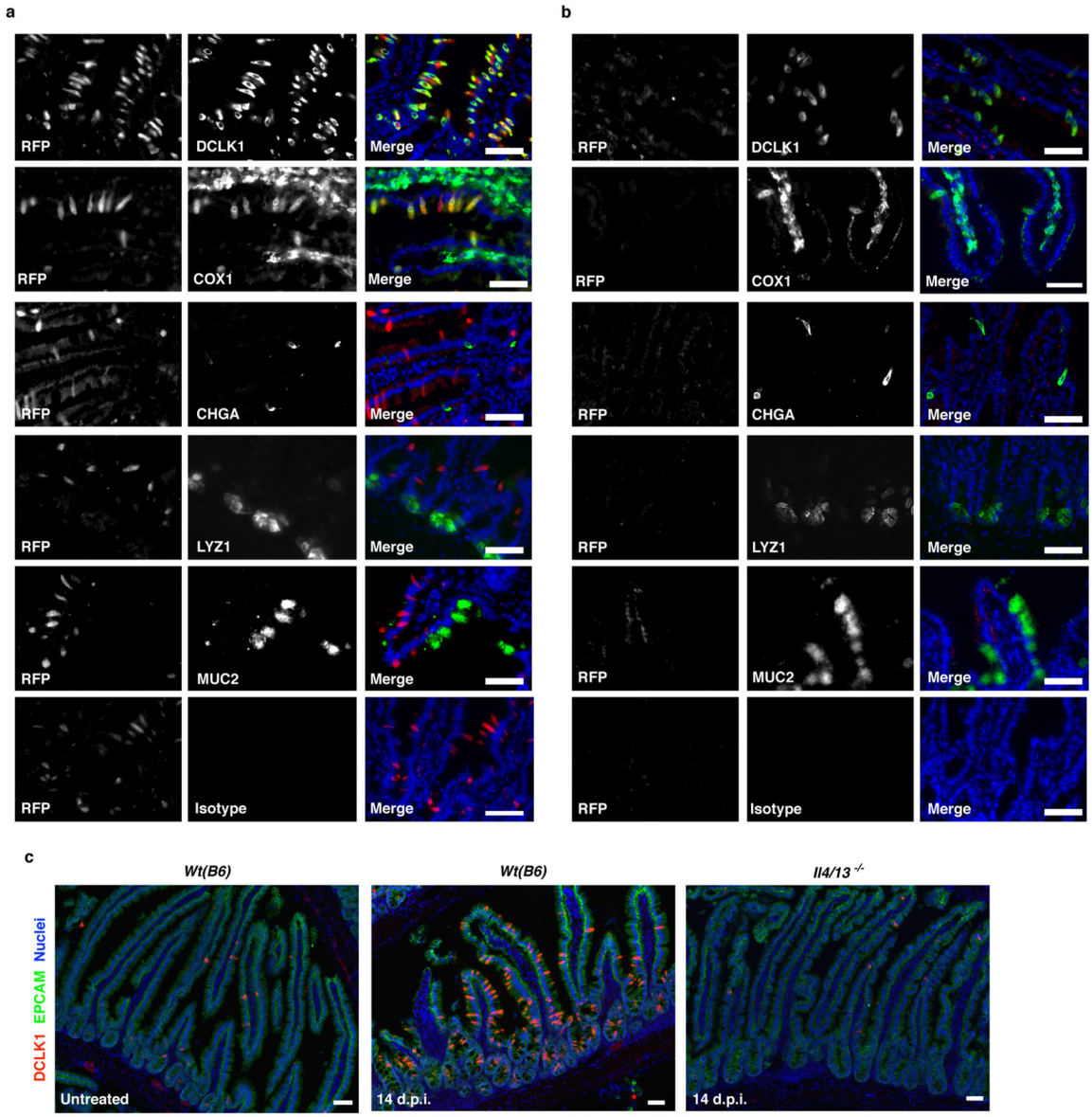

Extended Data Figure 7. *Il25* is expressed only in tuft cells during worm infection and *H. polygyrus* infection also induces tuft cell hyperplasia

a, **b**, Jejunum of *Il25*$^{F25/F25}$ (**a**) and wild-type control (**b**) mice infected for 7 days with *N. brasiliensis* stained by immunohistochemistry for RFP (red), indicated lineage markers (green), and DAPI (blue). **c**, Jejunum of indicated mice left untreated or infected 14 days with *H. polygyrus* and stained by immunohistochemistry for DAPI (blue), EPCAM (green) and DCLK1 (red). Scale bars, 50 μm. d.p.i., days post-*H. polygyrus* infection. Images are representative of one (**c**) or two (**a**, **b**) independent experiments. In **a**, **b**, n =2; in **c**, n = 1 (uninfected) or n =2 (infected).

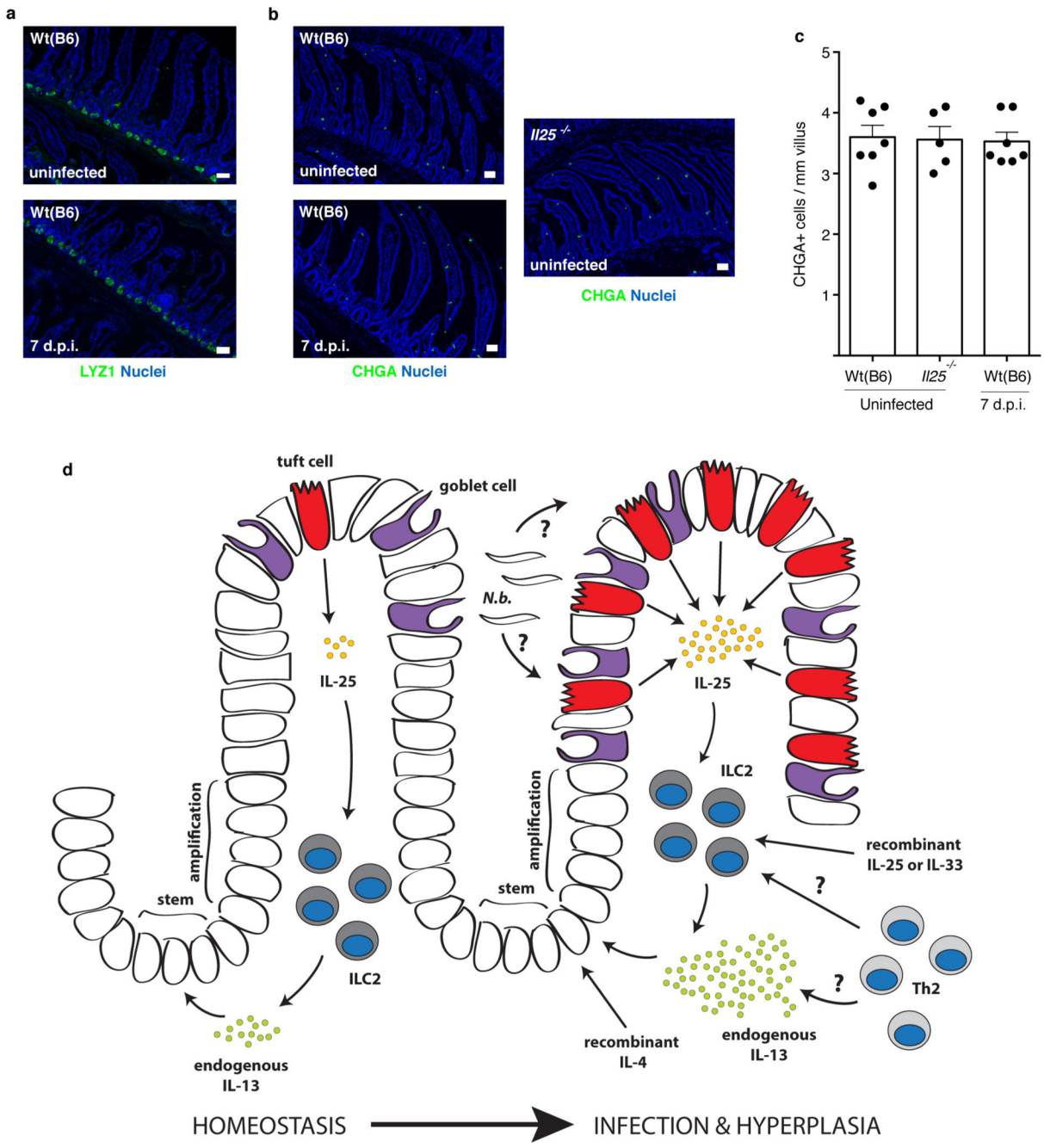

Extended Data Figure 8. Absence of Paneth and CHGA$^+$ cell hyperplasia after *N. brasiliensis* infection and model of ILC2–epithelial signalling circuit

a, **b**, Jejunum of indicated mice stained for DAPI (blue) and LYZ1/2 (**a**) or CHGA (**b**) (green). **c**, Quantification of CHGA$^+$ cells from imaging in (**b**). **d**, During homeostasis, rare epithelial tuft cells of the small intestine constitutively express *Il25*, which maintains low levels of IL-13 production in lamina propria ILC2s. IL-13 in turn signals uncommitted epithelial progenitors to promote emergence of tuft and goblet cells. In the absence of infection, this feed-forward ILC2–epithelial circuit is restrained by as yet unknown mechanisms. After *N. brasiliensis* (*N.b.*) infection, a helminth-derived signal or a change in

host physiology activates the ILC2–epithelial circuit leading to tuft and goblet cell hyperplasia and enhanced IL-13 production by ILC2s. Adaptive T_H2 cells probably also provide IL-13 and/or support ILC2 activation, especially when infection or inflammation lasts more than a week. Recombinant proteins are sufficient to induce tuft cell hyperplasia, either by inducing IL-13 production in lymphoid cells (IL-25 or IL-33) or by directly binding epithelial progenitors (IL-4). Scale bars, 50 μ m. d.p.i., days post-*N. brasiliensis* infection. Data in **c** are biological replicates. Data are representative of two (**a**) or three (**b**) independent experiments or pooled from multiple experiments (**c**). In **a**, *n* =2; in **b**, **c**, *n* is as shown in **c**. Error bars represent mean ±s.e.m.

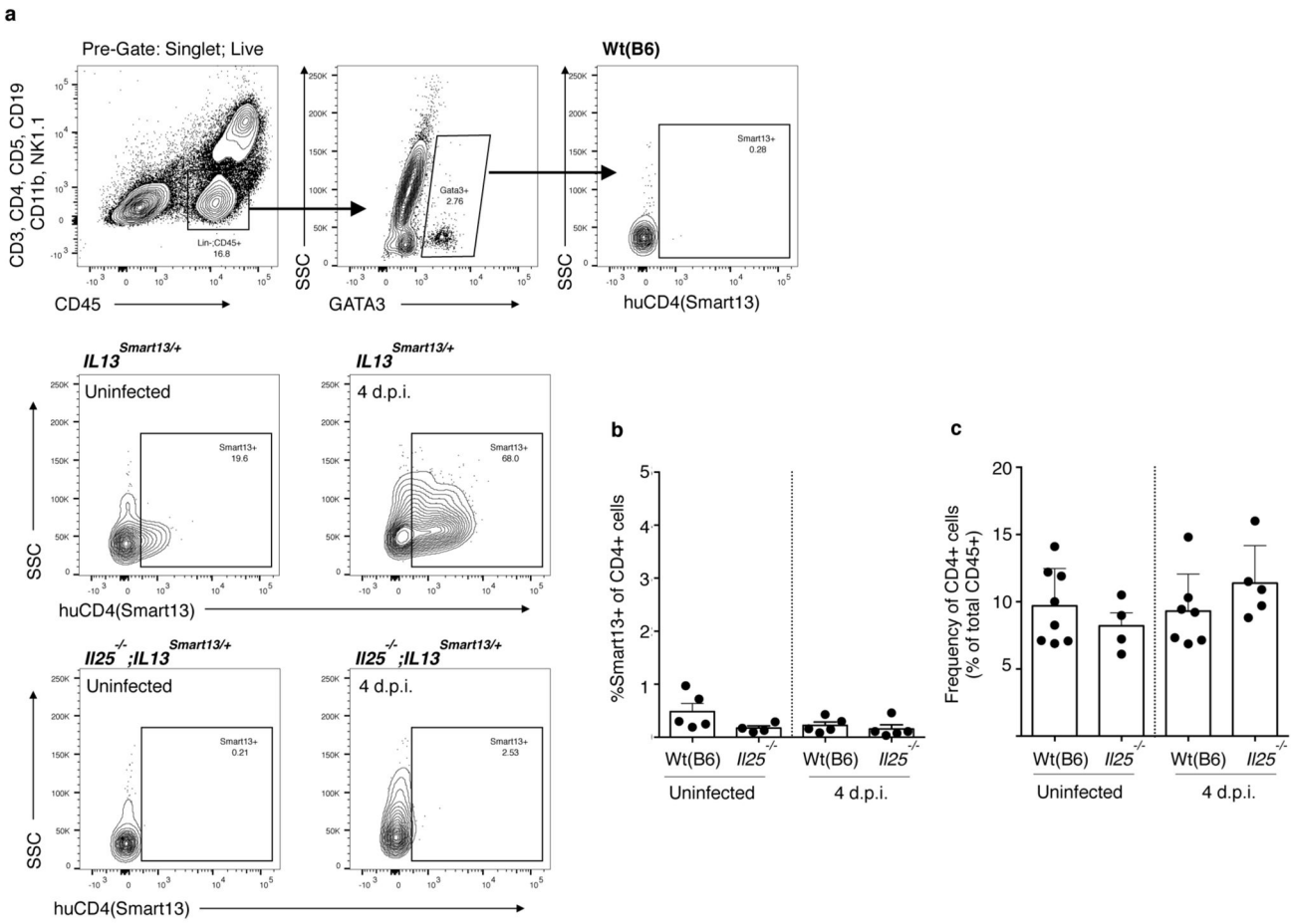

Extended Data Figure 9. IL-13 production by lamina propria ILC2 and CD4$^+$ cells

a, **b**, Lamina propria cells from *Il25*$^{-/-}$*;Il13*$^{Smart/+}$, *Il13*$^{Smart/+}$, and wild-type control mice analysed by flow cytometry and gated on ILC2 (**a**, Lin$^-$CD45$^+$GATA3$^+$) or CD45$^+$CD4$^+$ (**b**) cells. IL-13 secretion was quantified by measuring surface expression of human CD4, which is expressed from the *Il13* locus in *Il13*^{Smart} reporter mice. **c**, Frequency of lamina propria CD4$^+$ cells as a percentage of total CD45$^+$ cells as assessed by flow cytometry. d.p.i., days post-*N. brasiliensis* infection. Data in **b, c** are biological replicates. Data are representative of at least three (**a**) independent experiments, or pooled from multiple experiments (**b**, **c**). In **a**, *n* =5; in **b**, **c**, *n* is as shown. Error bars represent mean ±s.e.m.

Extended Data Table 1

Antibodies and quantitative RT–PCR primers used in this study

a

Immunohistochemistry Antibodies

Target	Conjugation	Host	Source	Dilution
dsRED	none	rabbit	Clontech (632496)	1:500
RFP	biotin	rabbit	Abcam (ab34771)	1:500
MUC2	none	rabbit	Santa Cruz (sc-15334)	1:100
LYS	none	rabbit	Dako (2017-06)	1:1000
CHGA	none	rabbit	Immunostar (20085)	1:250
DCLK1	none	rabbit	Abcam (ab31704)	1:1000
PTGS1	none	goat	Santa Cruz (sc-1754)	1:100
GFI1B	none	goat	Santa Cruz (sc-8559)	1:100
EPCAM	AF488	rat	Biolegend (G8.8)	1:250
KI67	AF488	rat	Biolegend (16A8)	1:100
rabbit IgG	AF488	goat	Life Technologies F(ab′)2	1:1000
rabbit IgG	AF555	goat	Life Technologies F(ab′)2	1:1000
rabbit IgG	AF488	chicken	Life Technologies F(ab′)2	1:1000
goat IgG	AF555	donkey	Life Technologies F(ab′)2	1:1000

b

Flow Cytometry Antibodies

Target	Conjugation	Source	Clone	Dilution
CD3	PerCP/Cy5.5	Biolegend	17A2	1:100
CD19	PerCP/Cy5.5	BD Biosciences	1D3	1:100
CD11B	PerCP/Cy5.5	Biolegend	M1/70	1:300
CD5	PerCP/Cy5.5	eBiosciences	53-7.3	1:1000
NK1.1	PerCP/Cy5.5	eBiosciences	PK136	1:100
EPCAM	PerCP/Cy5.5	Biolegend	G8.8	1:300
EPCAM	AF488	Biolegend	G8.8	1:300
GATA3	AF488	eBiosciences	TWAJ	2.5 μl/test
EPCAM	APC	Biolegend	G8.8	1:300
CD4	APC	BD Biosciences	RM4–5	1:100
CD45	BV605	Biolegend	30-F11	1:100
human CD4	PE	eBiosciences	RPA-T4	5 μl/test
DCLK1	none	Abcam		1:1000
rabbit IgG	AF488	Life Technologies		1:2000

c

qRT-PCR Primers

Target	Forward Primer (5′ -> 3′)	Reverse Primer (5′ -> 3′)
Dclk1	CAAGCCAGCCATGTCGTTC	TTCCTTTGAAGTAGCGGTCAC
Chga	ATCCTCTCTATCCTGCGACAC	GGGCTCTGGTTCTCAAACACT

c

qRT-PCR Primers

Target	Forward Primer (5′ -> 3′)	Reverse Primer (5′ -> 3′)
Chat	GGCCATTGTGAAGCGGTTTG	GCCAGGCGGTTGTTTAGATACA
Trpm5	TATGGCTTGTGGCCTATGGT	ACCAGCAGGAGAATGACCAG
Muc2	ATGCCCACCTCCTCAAAGAC	GTAGTTTCCGTTGGAACAGTGAA
Gnat3	TAGGAGCCGAGAGGACCAAG	GCTGGTATTCAGATGCCCTTTC
Lyz1	GAGACCGAAGCACCGACTATG	CGGTTTTGACATTGTGTTCGC
Lyz2	ATGGAATGGCTGGCTACTATGG	ACCAGTATCGGCTATTGATCTGA
Ptgs1	ATGAGTCGAAGGAGTCTCTCG	GCACGGATAGTAACAACAGGGA
Gfi1b	ATGCCACGGTCCTTTCTAGTG	GGAAGGCTCTGGTTCAGCAA
Il25	ACAGGGACTTGAATCGGGTC	TGGTAAAGTGGGACGGAGTTG
Tslp	ACGGATGGGGCTAACTTACAA	AGTCCTCGATTTGCTCGAACT
Il33	GCTGCGTCTGTTGACACATTGAG	GGTCTTGCTCTTGGTCTTTTCCAG
Rps17	CGCCATTATCCCCAGCAAG	TGTCGGGATCCACCTCAATG

Acknowledgments

We thank M. Consengco, R. Noyes, and Z. Wang for technical expertise, Y. Nusse for mice, members of the Locksley laboratory for helpful discussions, and R. Vance, M. Fontana, M. Anderson, and O. Klein for comments on the manuscript. This work was supported by the National Institutes of Health (AI026918, AI030663, HL107202), a Diabetes Endocrinology Research Center grant (DK063720), the Howard Hughes Medical Institute (HHMI), and the Sandler Asthma Basic Research Center at the University of California, San Francisco. J.v.M. is an HHMI Fellow of the Damon Runyon Cancer Research Foundation (DRG-2162-13).

References

1. Miller HR, Nawa Y. Immune regulation of intestinal goblet cell differentiation. Specific induction of nonspecific protection against helminths? Nouv Rev Fr Hematol. 1979; 21:31–45. [PubMed: 493106]
2. Castro GA, Badial-Aceves F, Smith JW, Dudrick SJ, Weisbrodt NW. Altered small bowel propulsion associated with parasitism. Gastroenterology. 1976; 71:620–625. [PubMed: 955350]
3. Grencis RK. Immunity to helminths: resistance, regulation, and susceptibility to gastrointestinal nematodes. Annu Rev Immunol. 2015; 33:201–225. [PubMed: 25533702]
4. Price AE, et al. Systemically dispersed innate IL-13-expressing cells in type 2 immunity. Proc Natl Acad Sci USA. 2010; 107:11489–11494. [PubMed: 20534524]
5. Neill DR, et al. Nuocytes represent a new innate effector leukocyte that mediates type-2 immunity. Nature. 2010; 464:1367–1370. [PubMed: 20200518]
6. Fallon PG, et al. Identification of an interleukin (IL)-25-dependent cell population that provides IL-4, IL-5, and IL-13 at the onset of helminth expulsion. J Exp Med. 2006; 203:1105–1116. [PubMed: 16606668]
7. Kang Z, et al. Epithelial cell-specific Act1 adaptor mediates interleukin-25-dependent helminth expulsion through expansion of $Lin^{-}c\text{-}Kit^{+}$ innate cell population. Immunity. 2012; 36:821–833. [PubMed: 22608496]
8. Zhao A, et al. Critical role of IL-25 in nematode infection-induced alterations in intestinal function. J Immunol. 2010; 185:6921–6929. [PubMed: 20974983]
9. Van Dyken SJ, et al. Chitin activates parallel immune modules that direct distinct inflammatory responses via innate lymphoid type 2 and γδ T cells. Immunity. 2014; 40:414–424. [PubMed: 24631157]

10. Owyang AM, et al. Interleukin 25 regulates type 2 cytokine-dependent immunity and limits chronic inflammation in the gastrointestinal tract. J Exp Med. 2006; 203:843–849. [PubMed: 16606667]
11. Angkasekwinai P, et al. Interleukin 25 promotes the initiation of proallergic type 2 responses. J Exp Med. 2007; 204:1509–1517. [PubMed: 17562814]
12. Clevers H. The intestinal crypt, a prototype stem cell compartment. Cell. 2013; 154:274–284. [PubMed: 23870119]
13. Bjerknes M, et al. Origin of the brush cell lineage in the mouse intestinal epithelium. Dev Biol. 2012; 362:194–218. [PubMed: 22185794]
14. Gerbe F, Legraverend C, Jay P. The intestinal epithelium tuft cells: specification and function. Cell Mol Life Sci. 2012; 69:2907–2917. [PubMed: 22527717]
15. Bezençon C, et al. Murine intestinal cells expressing Trpm5 are mostly brush cells and express markers of neuronal and inflammatory cells. J Comp Neurol. 2008; 509:514–525. [PubMed: 18537122]
16. McKenzie GJ, Bancroft A, Grencis RK, McKenzie ANJ. A distinct role for interleukin-13 in Th2-cell-mediated immune responses. Curr Biol. 1998; 8:339–342. [PubMed: 9512421]
17. Fort MM, et al. IL-25 induces IL-4, IL-5, and IL-13 and Th2-associated pathologies *in vivo*. Immunity. 2001; 15:985–995. [PubMed: 11754819]
18. Hurst SD, et al. New IL-17 family members promote Th1 or Th2 responses in the lung: *in vivo* function of the novel cytokine IL-25. J Immunol. 2002; 169:443–453. [PubMed: 12077275]
19. Liang HE, et al. Divergent expression patterns of IL-4 and IL-13 define unique functions in allergic immunity. Nature Immunol. 2012; 13:58–66. [PubMed: 22138715]
20. Voehringer D, Reese TA, Huang X, Shinkai K, Locksley RM. Type 2 immunity is controlled by IL-4/IL-13 expression in hematopoietic non-eosinophil cells of the innate immune system. J Exp Med. 2006; 203:1435–1446. [PubMed: 16702603]
21. Oliphant CJ, et al. MHCII-mediated dialog between group 2 innate lymphoid cells and $CD4^+$ T cells potentiates type 2 immunity and promotes parasitic helminth expulsion. Immunity. 2014; 41:283–295. [PubMed: 25088770]
22. Muñoz J, et al. The Lgr5 intestinal stem cell signature: robust expression of proposed quiescent '+4' cell markers. EMBO J. 2012; 31:3079–3091. [PubMed: 22692129]
23. Reinecker HC, Podolsky DK. Human intestinal epithelial cells express functional cytokine receptors sharing the common gamma c chain of the interleukin 2 receptor. Proc Natl Acad Sci USA. 1995; 92:8353–8357. [PubMed: 7667294]
24. Nussbaum JC, et al. Type 2 innate lymphoid cells control eosinophil homeostasis. Nature. 2013; 502:245–248. [PubMed: 24037376]
25. Deckmann K, et al. Bitter triggers acetylcholine release from polymodal urethral chemosensory cells and bladder reflexes. Proc Natl Acad Sci USA. 2014; 111:8287–8292. [PubMed: 24843119]
26. Krasteva G, et al. Cholinergic chemosensory cells in the trachea regulate breathing. Proc Natl Acad Sci USA. 2011; 108:9478–9483. [PubMed: 21606356]
27. Saunders CJ, Christensen M, Finger TE, Tizzano M. Cholinergic neurotransmission links solitary chemosensory cells to nasal inflammation. Proc Natl Acad Sci USA. 2014; 111:6075–6080. [PubMed: 24711432]
28. Lee RJ, et al. Bitter and sweet taste receptors regulate human upper respiratory innate immunity. J Clin Invest. 2014; 124:1393–1405. [PubMed: 24531552]
29. Ballantyne SJ, et al. Blocking IL-25 prevents airway hyperresponsiveness in allergic asthma. J Allergy Clin Immunol. 2007; 120:1324–1331. [PubMed: 17889290]
30. Han H, Thelen TD, Comeau MR, Ziegler SF. Thymic stromal lymphopoietin-mediated epicutaneous inflammation promotes acute diarrhea and anaphylaxis. J Clin Invest. 2014; 124:5442–5452. [PubMed: 25365222]
31. Sato T, Clevers H. Primary mouse small intestinal epithelial cell cultures. Methods Mol Biol. 2013; 945:319–328. [PubMed: 23097115]

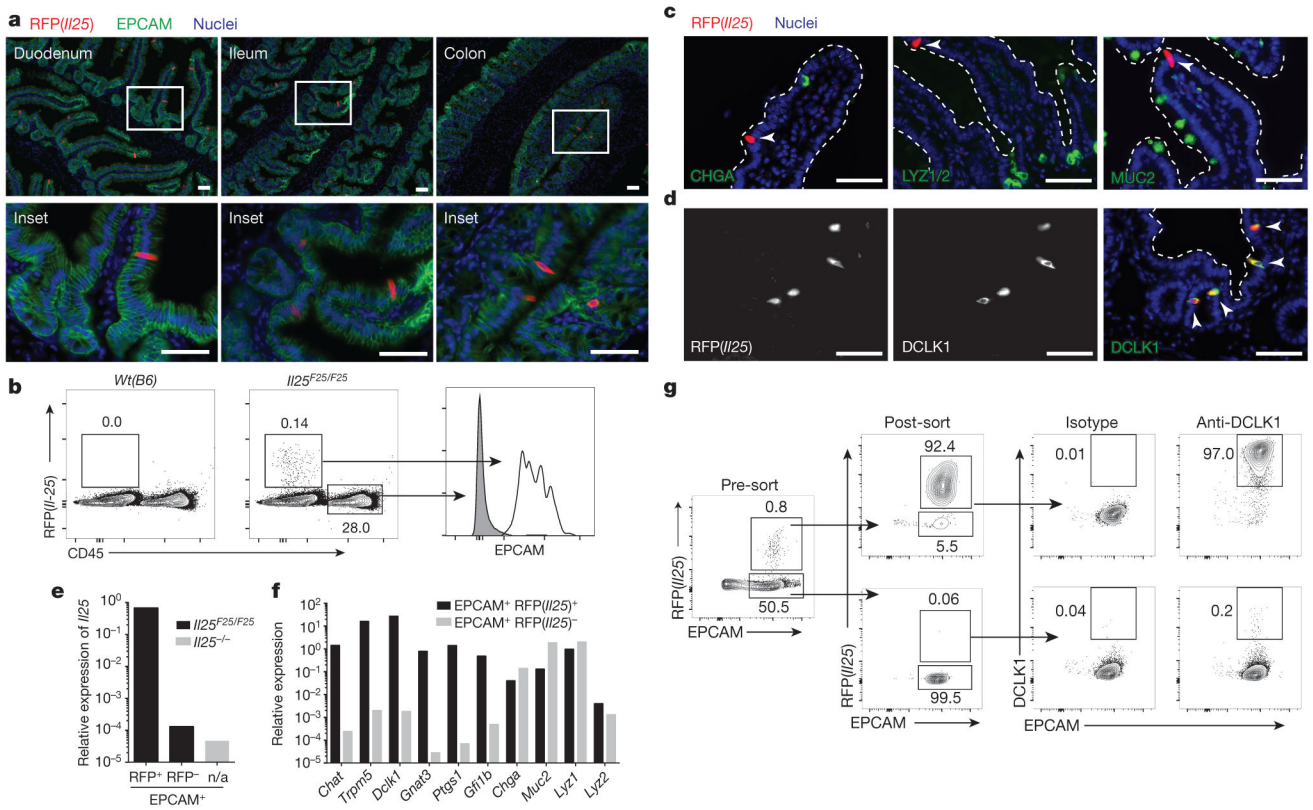

Figure 1. Intestinal tuft cells constitutively express *Il25*

a, Indicated tissues from *Il25*$^{F25/F25}$ mice stained for RFP (red), EPCAM (green) and 4′,6-diamidino-2-phenylindole (DAPI; blue). **b**, Flow cytometry of digested jejunum. **c**, **d**, Jejunum from *Il25*$^{F25/F25}$ mice stained as indicated. Dotted lines outline villi. Arrowheads indicate RFP^{+} cells. **e**, **f**, Quantitative polymerase chain reaction with reverse transcription (RT–PCR) on cells sorted from small intestines of *Il25*$^{-/-}$ (**e**) and *Il25*$^{F25/F25}$ (**e**, **f**) mice. n/a, not applicable. **g**, Flow cytometry of cells sorted from small intestines of *Il25*$^{F25/F25}$ mice and stained with anti-DCLK1. Scale bars,350 μm. All data are biological replicates. Data are representative of two (**b–d, g**), or at least three (**a**, **e**, **f**) experiments. In **a**, n >5; in **b–d**, **g**, n =2; in **e**, **f**, n =3.

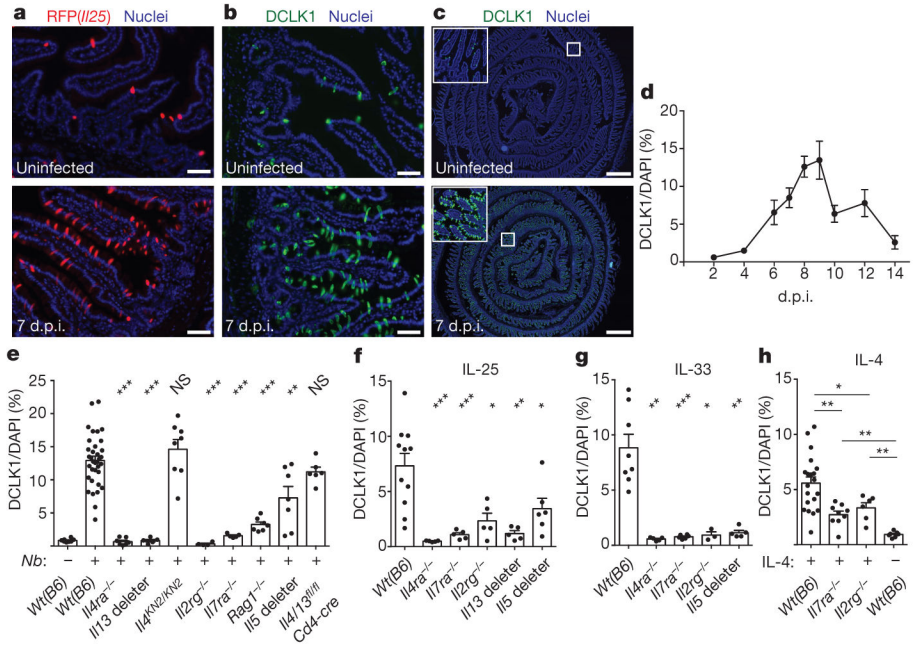

Figure 2. Worm infection induces IL-13-dependent tuft cell hyperplasia

a–**c**, Jejunum from *Il25*$^{F25/F25}$ mice stained for RFP (**a**) or DCLK1 (**b**, **c**). **d**–**h**, Immunohistochemical quantification of tuft cells (DCLK1^{+}) in duodenum/jejunum of mice infected with *N. brasiliensis* for indicated days (**d**) or 7 days (**e**) or injected with indicated protein (**f**–**h**). Scale bars: 50 μm (**a**, **b**), 1 mm (**c**). All data are biological replicates. Data are representative of at least three (**a**–**c**) experiments or pooled (**d**–**h**) from multiple experiments. In **a**–**c**, n >10; in **d**, day 2: n = 2; days 4, 12, 14: n = 4; day 9: n = 5; days 6, 8, 10: n = 6; day 7: n =8; in **e**–**h**, n is as shown. *Nb*, *N. brasiliensis*. *P <0.05; **P <0.01, ***P < 0.001; NS, not significant (Mann–Whitney test). Error bars represent mean ±standard error of the mean (s.e.m.).

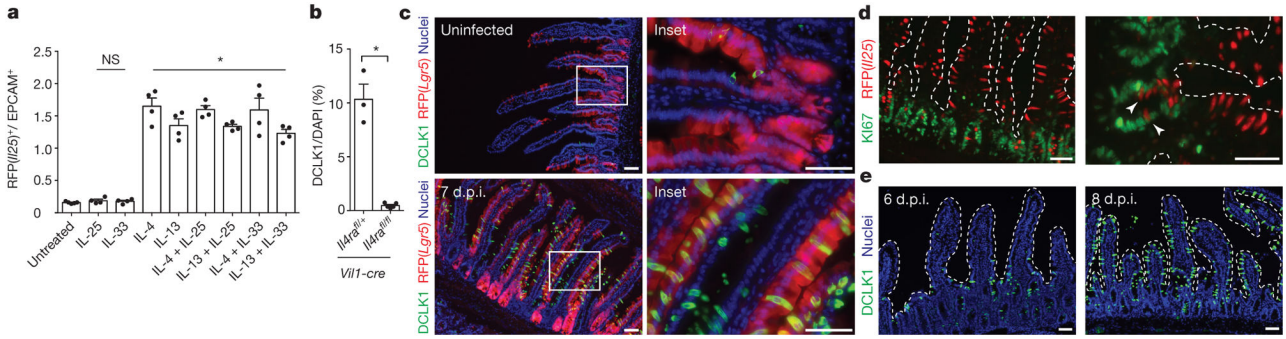

Figure 3. IL-13 signalling in epithelial progenitors gives rise to tuft cell hyperplasia

a, Flow cytometric quantification of RFP^{+} tuft cells in intestinal organoids grown from *Il25*$^{F25/F25}$ mice and treated with indicated recombinant proteins (20 ng ml^{-1}). **b**, Immunohistochemical quantification of tuft cells (DCLK1^{+}) in duodenum/jejunum of mice infected 7 days with *N. brasiliensis*. **c**, Jejunum of *Lgr5*$^{cre\text{-}Ert2/+}$; *Gt(ROSA)26*$^{STOP\text{-}flox::RFP/+}$ mice treated 5 days with tamoxifen and stained for DCLK1 (green) and DAPI (blue). *N. brasiliensis* infection as indicated. **d**, **e**, Jejunum of *Il25*$^{F25/F25}$ (**d**) or *Wt(B6)* (**e**) mice infected for 7 days (**d**) or indicated number of days (**e**) with *N. brasiliensis* and stained for RFP (red) and Ki67 (green) (**d**) or DCLK1 (green) and DAPI (blue) (**e**). **d**, **e**, Dotted lines outline villi. Scale bars, 50 μm. Arrowheads indicate Ki67 and RFP overlap. Data in **a** are technical replicates, all other data are biological replicates. Data are representative of two (**c**–**e**) or three (**a**) experiments or pooled (**b**) from multiple experiments. In **a**, **b**, *n* is as shown; in **c**, uninfected: *n* =4; 7 d.p.i.: *n* =5; in **d**, *n* =2; in **e**, *n* =4. *Nb*, *N. brasiliensis*. *$P < 0.05$; NS, not significant (Mann–Whitney test). Error bars represent mean ±s.e.m.

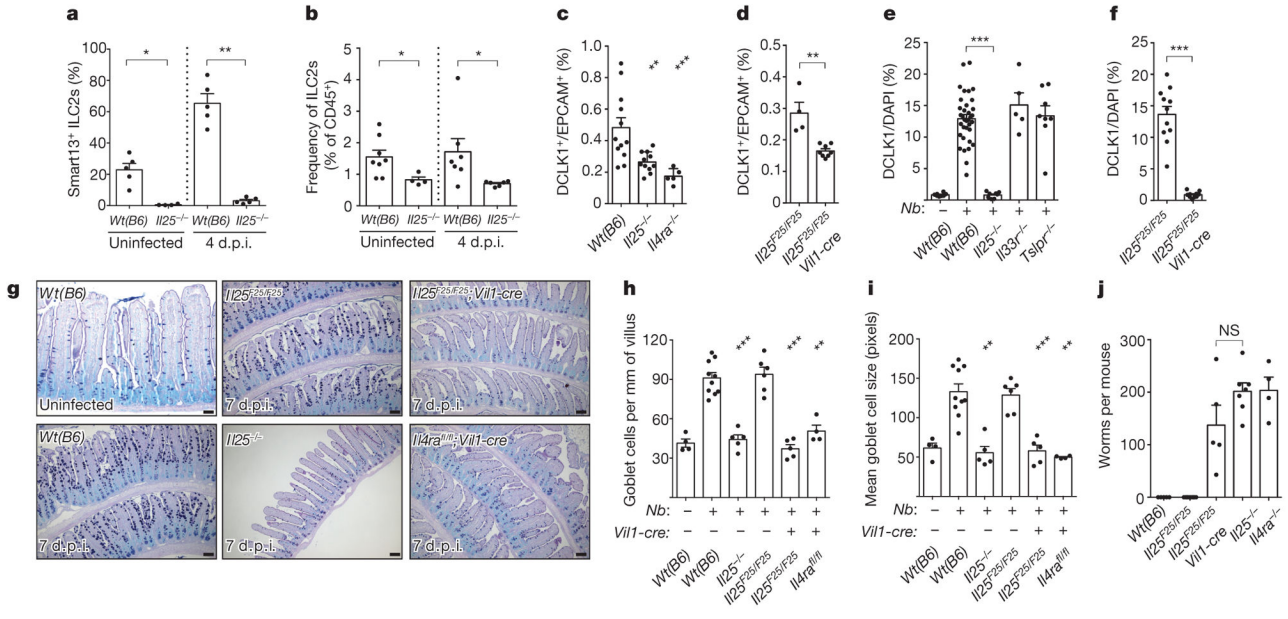

Figure 4. Tuft cells regulate intestinal physiology through an ILC2–epithelium response circuit

a, **b**, Flow cytometric analysis of lamina propria ILC2s (Lin^-, $CD45^+$, $GATA3^+$) from *Il13*$^{Smart/+}$ and *Il25*$^{-/-}$*;Il13*$^{Smart/+}$ mice. **c**, **d**, Flow cytometric quantification of tuft cells ($DCLK1^+$) in jejunum of uninfected mice. **e**, **f**, Immunohistochemical quantification of tuft cells ($DCLK1^+$) in jejunum/duodenum of mice infected 7 days with *N. brasiliensis.* In **e**, wild-type controls are the same as in Fig. 2e. **g**, Jejunum of mice treated as indicated and stained for goblet cells with periodic acid Schiff (PAS) Alcian blue. **h**, **i**, Goblet cell number (**h**) and size (**i**) calculated from imaging. **j**, Intestinal worm burden in mice infected 10 days with *N. brasiliensis.* Scale bars, 50 μm. All data are biological replicates. Data are representative of two (**g**) experiments or pooled (**a**–**f**, **h**–**j**) from multiple experiments. In **g**, *n* is as shown in **h** and **i;** in **a**–**f**, **h**–**j**, *n* is as shown. *Nb*, *N. brasiliensis.* **P* <0.05; ***P* <0.01; ****P* < 0.001; NS, not significant (Mann–Whitney test). Error bars represent mean ±s.e.m.